

Advantage of Fractional Calculus Based Hybrid-Theoretical-Computational-Experimental Approach for Alternating Current Voltammetry

Saurav K. Guin,^{*,[a]} Arvind S. Ambollikar,^[a, b] Shantanu Das,^[c] and Ashwini K. Poswal^[d]

Abstract: The dynamic electrochemical behavior of electroactive species is believed to be represented better by the fractional calculus, because it can consider the history of mass-transfers of that species near the electrode surface. The elucidation of mathematical fundamentals of fractional calculus has been recently introduced for batteries, supercapacitors and a few voltammetry studies. The working equations for faradaic fundamental and second-harmonic (SHac) components of alternating current (ac) for ac voltammetry of an electrochemically reversible redox reaction on an electrode of macroscopic diameter have been derived here by using generalized formulae of the fractional calculus. A computation code is written in Python language with a matrix based algorithm

Keywords: AC Voltammetry · Theory-Computation-Experiment · Fractional Calculus · Faradaic Current · Python Computation Language

developed based on latest, accurate, efficient and stable Grunwald-Letnikov-Improved fractional-order differentiation equation. That computational code is used to find the concealed faradaic fundamental, SHac components of the total current and other double-layer parameters of experimentally recorded voltammograms of ruthenium (III/II) redox reaction on gold-disc electrode by a common electrochemical workstation without having inbuilt Fourier transformation features. The amplitude of the computed faradaic current concealed in the experimental data gets enhanced through this hybrid theoretical-computational-experimental approach and thus it keeps scope of application and further improvement in electroanalysis.

1 Introduction

Voltammetry is a suite of electrochemical techniques widely used to characterize the thermodynamics, kinetics and mechanism of the heterogeneous electron transfer reaction of a molecule, ion or complex of interest (hereafter will be referred as analyte) occurring at the working electrode (WE). A couple of important electrochemical parameters such as formal redox potential (E'_0), electron transfer coefficient (α_c) and standard heterogeneous electron transfer rate constant (k_0) of an electrochemically reversible reaction can be calculated through cyclic voltammetry (CV) from the measured current ($i(t)$) with respect to the linearly varied (with time (t)) potential ($E(t)$) at high perturbations (up to few hundreds of mV) to both higher and lower potentials with respect to E'_0 . In CV, the capacitive ($i_c(t)$) current resulted from the double layer capacitance (C_{DL}) sometimes hides the prominence of the faradaic ($i_f(t)$) current of interest. On the other hand, the electrochemical impedance spectroscopy (EIS) slightly (by 5–10 mV) perturbs $E(t)$ sinusoidally around a base potential of interest (most commonly at the open circuit potential or at E'_0) with different angular frequencies (ω ; where $\omega = 2\pi f$ and f is the linear frequency). It decouples the electrochemical processes of different time constants occurring at the electrode-electrolyte interface at that base potential of interest and provides information about respective charge transfer resistance (R_{CT}), C_{DL} and

diffusion coefficients related parameter such as Warburg coefficient (σ_w). However, it fails to provide the complete information about the variation of those interfacial parameters with the potentials, unless repeating the same experiment at different base potentials. The potentiodynamic impedance spectroscopy is a special experimental technique useful for this purpose, but it is not very popular owing to the need of rigorous data analysis. The alternating current (ac) voltammetry has the quality to unify the positive outcomes of CV and EIS in wide range

[a] Dr. S. K. Guin, A. S. Ambollikar
Fuel Chemistry Division, Bhabha Atomic Research Centre,
Trombay, Mumbai – 400085, India
Tel.: +91-22-2559-4591
Fax: +91-22-2550-5151
E-mail: sauravkrguin@yahoo.co.in
skguin@barc.gov.in

[b] A. S. Ambollikar
Homi Bhabha National Institute, Anushakti Nagar, Mumbai –
400094, India

[c] S. Das
Reactor Control System Design Section, Bhabha Atomic Research
Centre, Trombay, Mumbai – 400085, India

[d] A. K. Poswal
Atomic & Molecular Physics Division, Bhabha Atomic Research
Centre, Trombay, Mumbai – 400085, India

Supporting information for this article is available on the
WWW under <https://doi.org/10.1002/elan.201900552>

of potential of interest. In ac voltammetry, a sinusoidal potential perturbation of a particular ω and small amplitude (ΔE) is superimposed over $E(t)$, which linearly varies with t . The research and development on ac polarography/voltammetry started almost fifty years ago by few research groups [1–5]. The research was then extended to explore the utilization of Fourier transformation in ac voltammetry [6–11]. Special microprocessor based instrumentations and simulation techniques were developed to utilize it in real systems [12–19]. Hence, the experimental and theoretical explorations were spread over different natures and amplitude of perturbation signals and ramp of base potentials [20–25]. This special instrumentation of Fourier transformed ac voltammetry has been used to understand many electrochemical phenomena [26–35]. In parallel, several other mathematical approaches have been initiated with some basic assumptions to explore ac voltammetry by series functions [10], Bessel functions [36–38], convolutions [39] and semi-integrals [40–52]. However, the popularity of ac voltammetry has not met the levels of CV and EIS due to the comparatively complex theoretical modeling and analysis of the experimental data.

The classical calculus developed by Newton and Leibniz deals with the differentiation and integration of integer orders. The fractional calculus is more general because it has the ability to deal with both the integer and non-integer order of operations. The classical differentiation is defined for a function at a point of interest of the independent variable. On the contrary, the operation of fractional order differentiation is non-local as it requires all the previous history of the function at all the values of the independent variable till the point of interest. The classical integration represents the area under a curve defined by a function where we actually take a sum of the infinitesimal slices of areas of fixed weightage in the finite interval of the independent variable. On the other hand, the fractional-order integration represents the area under a curve whose shape keeps on changing as well as the weightage of each infinitesimal slice of areas under the curve changes in a definite interval of the independent variable. The concept of fractional calculus was thought by Leibniz in 1695 and the related theories have been developed by several mathematicians over more than 300 years. For many years, the evolution of fractional calculus was mostly restricted into abstract mathematical sciences, but its importance in the applied science and engineering has been recently realized [53–55]. The importance of differential equations of fractional-orders in electrochemistry has been realized in 2010 [48]. The models for suitable equivalent electrical circuits for supercapacitors and batteries are being developed through fractional calculus [56–62]. The exploration of the use of fractional calculus in voltammetry is also recently initiated [63, 64]. In voltammetry, $i(t)$ is proportional to the gradient ($J_{x=0,t}$) of the concentration of analyte at electrode surface ($x=0$) at time t , but actually $i(t)$ holds the history of variation of $J_{x=0,t}$ with t . Therefore, $i(t)$ should be represented by the

fractional calculus of a function related to the concentration of analyte at the interface. The idea of fractional calculus in voltammetry was introduced in almost similar times in different names by Oldham's group as semi-differentiation where 'semi' denotes $\frac{1}{2}$ [39, 42, 45, 49, 51, 52] and Saveant's group as convolution integrals [26, 65–68]. The differintegration term represents a combined differentiation and integration operation frequently encountered in the fractional calculus [55]. The voltammetric analysis is inherently restricted to $\frac{1}{2}$ -order calculus (Eq. S12 and S13 as developed in Appendix-S1 in the *Supporting Information File*) as the general mass-flow of the analyte in voltammetry is obeyed by the Fick's laws of diffusion. The 'semi-calculus' has recently been employed to model the CV and aperiodic component of ac voltammogram [45, 49, 50, 63, 69]. These two independent approaches of similar central idea but with different names are basically limited portions of the broader view of fractional calculus, because semi-differentiation is specified only to order 0.5 and the integro-differential equations of fractional calculus deal with convolution type of integrals. On the other hand, there is a recent trend to develop computational tools and algorithms for fractional calculus of any order to meet its applications in science and technology [70–73].

Therefore, it was of our prime interest, to present a fresh perspective based on the generalized theories and equations of fractional calculus to derive the working equations of fundamental and second-harmonic ac voltammetry of an electrochemically reversible redox reaction on a macro-disc WE as the simple point of initiation. In this direction, it was observed that the current-semi-integral had been used in the literature to derive the general *Faraday-Fick-Butler-Volmer Equation* or commonly known as *Pan-Voltammetric Relation* for an electrochemically reversible redox reaction [74]. The current-semi-integral was used there to express the surface concentrations of the oxidized (O) and reduced (R) states of the species, which were used to finally derive the R_{CT} and σ_w followed by the in-phase faradaic component of ac. We followed a similar initial approach to derive the expression of the surface concentrations of O and R by the semi-integral. Thereafter, we followed a different mathematical approach based on the Taylor Series expansion of the semi-integral, itself, to derive the complete expressions (*Section 1.1*) for the dc, fundamental (Fac) and second-harmonic (SHac) components of ac quite different from those reported earlier. Then we have included the effect of other cell components such as C_{DL} , R_{CT} , uncompensated resistance (R_u), etc. to the faradaic process to derive the expressions of the experimentally recordable in-phase (IP) and out-of-phase (OP) components of the ac (*Section 1.2*). Further, we expanded our motivation to build-up a suitable commercially free computer program written in Python language (*Section 2.1*) to numerically operate the derived working equations based on fractional calculus on the experimental data recorded for the electrochemically reversible

redox reaction of hexaammineruthenium(III)/(II) chloride ($[\text{Ru}(\text{NH}_3)_6]^{3+/2+}$) in potassium chloride (KCl) on gold (Au) disk electrode of macroscopic diameter as a function of amplitude and frequency of sine perturbation generated by a simple electrochemical workstations commonly available in many labs (Section 2.2) [75,76]. Several check-points have been set-up to confirm the authenticity of the above mentioned computation process. During this computational process for calculating the concealed faradaic current from the experimental data, the singularity issue was unavoidable and thus another hybrid computational-experimental was also evolved during that process. Further, the experimental data recorded during the process for the above-mentioned electrochemical reaction could provide valuable features of some electrochemical interfacial parameters such as double layer capacitance, faradaic impedance and phase-difference between the signal and response in the wide range of electrochemical potentials.

1.1 Derivation of General Working Equations

The semi-integral ($m_0(t, \omega)$) is related with the applied ac signal ($E(t, \omega)$) through reversible Pan-Voltammetric Relation (Eq. S19, S20) as derived in Appendix-S2 in the Supporting Information File. The ac voltammetry experiment actually happens in quasi-time state, that means in-phase ($i_{m-ac-IP}(t, \omega)$) and out-of-phase ($i_{m-ac-OP}(t, \omega)$) currents at ω are sampled by lock-in-amplifier for a time (t_{smp}) at each base potential, $E_b(t, \omega)$, which linearly varies with t . Therefore, we could assume that the electrochemical reaction remains in quasi-equilibrium state at each $E(t, \omega)$ (or equivalently at each $E_b(t, \omega)$) and the sine potential perturbation, $p(t, \omega)$, applied on $E(t, \omega)$ generates ac response of the electrochemical reaction. Therefore, the total semi-integral, $m(t, \omega)$ at $E(t, \omega)$ can be expressed by Taylor's series (Eq. 1–3):

$$m(t, \omega) = m_0(t, \omega) + m'_0(t, \omega)p(t, \omega) + \frac{1}{2!}m''_0(t, \omega)(p(t, \omega))^2 + \dots \quad (1)$$

where,

$$m'_0(t, \omega) = \frac{dm_0(t, \omega)}{dE(t, \omega)} = \frac{dm_0(t, \omega)}{dt} \times \frac{dt}{dE(t, \omega)} \quad (2)$$

and

$$m''_0(t, \omega) = \frac{d^2m_0(t, \omega)}{dE(t, \omega)^2} = \frac{dm'_0(t, \omega)}{dt} \times \frac{dt}{dE(t, \omega)} \quad (3)$$

The first, second and third terms in the right hand side of Eq. 1 represent the direct (dc) [$m_0(t, \omega)$], fundamental (F-) [$m_1(t, \omega)$] and second harmonic (SH-) [$m_2(t, \omega)$] components, respectively, of $m(t, \omega)$ in ac voltammetry. The fractional differentiation (${}_0D_t^{\frac{1}{2}}$) of $m_0(t, \omega)$ with

respect to t leads to $i_{dc}(t, \omega)$, which has almost no influence of alternating pulse and it is the current response almost similar to linear scan voltammetry [77–80].

$$i_{dc}(t, \omega) = nFA\sqrt{D_{O0}}D_t^{\frac{1}{2}}[m_0(t, \omega)] = -nFA\sqrt{D_{O0}}C_O^*\chi(t, \omega) \quad (4)$$

where,

$$\chi(t, \omega) = \frac{1}{2\sqrt{\pi}} \left[\frac{1}{\sqrt{t}} + 4 \sum_{k=\pi}^{\infty} \left\{ \frac{\sqrt{k^2 + (d-\Delta)^2} + 2d - 2\Delta}{(k^2 + (d-\Delta)^2)^{\frac{3}{2}}} \sqrt{\frac{\sqrt{k^2 + (d-\Delta)^2} - d + \Delta}{8}} \arccos\left(\frac{\sqrt{k^2 + (d-\Delta)^2} - d}{\sqrt{k^2 + \Delta^2}}\right) + \frac{\sqrt{k^2 + (d-\Delta)^2} - 2d + 2\Delta}{(k^2 + (d-\Delta)^2)^{\frac{3}{2}}} \sqrt{\frac{\sqrt{k^2 + (d-\Delta)^2} + d - \Delta}{8}} \arccos\left(\frac{\sqrt{k^2 + (d-\Delta)^2} + d}{\sqrt{k^2 + \Delta^2}}\right) + \frac{d - \Delta}{(k^2 + (d-\Delta)^2)\sqrt{d}} \right\} \right] \quad (5)$$

with, $\Delta = \frac{nF}{RT}(E_i - E_{\frac{1}{2}})$; $E_{\frac{1}{2}} = E'_0 - \frac{RT}{2nF} \ln\left(\frac{D_O}{D_R}\right)$ and $d = \frac{nF}{RT}(vt + \Delta E \sin \omega t)$. The detail derivation of Eq. 5 is shown in Appendix-S3 in the Supporting Information File.

Similarly, the faradaic fundamental ac component ($i_{f-ac}[t, \omega]$) at $E(t, \omega)$ can be calculated by fractional differentiation (${}_0D_t^{\frac{1}{2}}$) of $m_1(t, \omega)$ with respect to t :

$$i_{f-ac}[t, \omega] = M_1(t, \omega) \sin\left(\omega t + \frac{\pi}{4}\right) \quad (6)$$

where, the amplitude ($M_1(t, \omega)$) of the $i_{f-ac}[t, \omega]$ has a complicated dependency on ΔE , ω and v as expressed in Eq. 7.

$$M_1(t, \omega) = -\frac{n^2F^2A\Delta EC_O^*\sqrt{D_{O0}\omega}}{4RT} \operatorname{sech}^2\left[\frac{nF}{2RT}\{E(t, \omega) - E_{\frac{1}{2}}\}\right] \quad (7)$$

and $M_1(t, \omega)$ is maximum at $E(t, \omega) = E_{\frac{1}{2}}$. Further, $i_{f-ac}[t, \omega]$ has phase difference of ($+45^\circ$) with respect to the applied sine perturbation. The steps of derivation of Eq. 6 are shown in Appendix-S4 in the Supporting Information File.

The faradaic second-harmonic ac component ($i_{f-ac}[t, 2\omega]$) at $E(t, \omega)$ can be calculated by fractional

differentiation (${}_0D_t^{\frac{1}{2}}$) of $m_2(t, \omega)$ with respect to t and considering the second-harmonic components with high-pass frequency (2ω) as Eq. 8.

$$i_{f-ac}[t, 2\omega] = nFA\sqrt{2\omega D_O}X_2(t, \omega)\sin\left(2\omega t - \frac{\pi}{4}\right) \quad (8)$$

where,

$$X_2(t, \omega) = -\frac{n^2F^2C_O^*\Delta E^2}{16R^2T^2} \sinh\left[\frac{nF}{2RT}\{E(t, \omega) - E_{\frac{1}{2}}\}\right] \operatorname{sech}^3\left[\frac{nF}{2RT}\{E(t, \omega) - E_{\frac{1}{2}}\}\right] \quad (9)$$

The main steps are shown in Appendix-S5 in the *Supporting Information File*. The $i_{f-ac}[t, \omega]$ and $i_{f-ac}[t, 2\omega]$ represent the faradaic fundamental and second-harmonic components of the ac voltammetry of an electrochemically reversible reaction in the influence of applied potential signal. Although, Eq. 4, 6 and 8 represent the popular expressions of the dc, fundamental and second harmonic components of faradaic ac currents; their actual forms as mentioned in the derivation steps and related assumptions mentioned therein hold the keys to explore, in future, the anomalies between the experimental and expected data, if any.

1.2 Derived Parameters to Correlate Theory with Experiment

We cannot directly measure $i_{f-ac}[t, \omega]$ and $i_{f-ac}[t, 2\omega]$ through any electrochemical experiment. In the electrochemical cell, the measured fundamental ac component ($i_{m-ac}[t, \omega]$) is actually consists of $i_{f-ac}[t, \omega]$ and the capacitive ac component ($i_{c-ac}[t, \omega]$), which originates from the molecular or ionic reorganization at the electrode-electrolyte interface under the influence of the applied potential signal. The phase sensitive detector of the general potentiostat measures the in-phase ($i_{m-ac-IP}(t, \omega)$) and out-of-phase ($i_{m-ac-OP}(t, \omega)$) components of $i_{m-ac}[t, \omega]$ in synchronization with t . One can easily calculate $M_1(t, \omega)$, faradaic impedance ($Z_f(t, \omega)$), $X_1(t, \omega)$, $m_1(t, \omega)$ and $i_{f-ac}[t, \omega]$ from $i_{m-ac-IP}(t, \omega)$ by using Eq. S71–S73 (important steps are available in Appendix-S6). Further, we could study the variation in the surface concentrations of O and R i.e.; $C_O(0, t, \omega)$ and $C_R(0, t, \omega)$ through the fundamental component of ac voltammetry by Eq. S16. Notably, those parameters are difficult to measure directly from experiments.

On the other hand, the harmonics of the electrochemical response are in-situ generated at the electrode-electrolyte interface by the faradaic elements [46]. Therefore, the second harmonic ac component $i_{m-ac}[t, 2\omega]$ is measured across the uncompensated resistance (R_u) existing at the in-situ potential drop $p(t, 2\omega)$, i.e.; $p(t, 2\omega) = -\Delta E \sin 2\omega t$. Since, we are not able to confirm

that the double layer capacitances for fundamental and second harmonic are identical, hence we are representing the double layer capacitance involved in the SHac voltammetry as $C_{DL}(t, 2\omega)$. If we define the time constant, $T(t, 2\omega) = R_u C_{DL}(t, 2\omega)$. The measured in-phase ($i_{m-ac-IP}(t, 2\omega)$) and out-of-phase ($i_{m-ac-OP}(t, 2\omega)$) components of SHac voltammogram are represented by Eq. 10, respectively. (Important steps are available in Appendix-S7 in the *Supporting Information File*)

$$\left. \begin{aligned} i_{m-ac-IP}(t, 2\omega) &= \frac{nFAD_O^{\frac{1}{2}}X_2(t, \omega)\omega^{\frac{1}{2}}}{(1+4\omega^2T(t, 2\omega)^2)} \{1 - 2\omega T(t, 2\omega)\} \\ i_{m-ac-OP}(t, 2\omega) &= -\frac{nFAD_O^{\frac{1}{2}}X_2(t, \omega)\omega^{\frac{1}{2}}}{(1+4\omega^2T(t, 2\omega)^2)} \{1 + 2\omega T(t, 2\omega)\} \end{aligned} \right\} \quad (10)$$

Inspecting Eq. 10, it can be said that $i_{m-ac-IP}(t, 2\omega)$ and $i_{m-ac-OP}(t, 2\omega)$ will be equal only at $X_2(t, \omega) = 0$ i.e., at $E(t, \omega) = E_{\frac{1}{2}}$ (Eq. 9). The measured amplitude of the second harmonic ac component ($|i_{m-ac}(t, 2\omega)|$) at $E(t, \omega)$ is represented by Eq. S76 and it will be zero at $E(t, \omega) = E_{\frac{1}{2}}$ because at that point $X_2(t, \omega) = 0$. The phase shift ($\varphi_{SH}(\text{degree})$) between the $E(t, \omega)$ and $i_{m-ac}[t, 2\omega]$ in four-quadrants is given by Eq. S77 and the phase of $i_{m-ac}[t, 2\omega]$ will be shifted by 270° at $E(t, \omega) = E_{\frac{1}{2}}$. If we can calculate $X_2(t, \omega)$ from $i_{m-ac-IP}(t, 2\omega)$ and $i_{m-ac-OP}(t, 2\omega)$ through algebraic equations (Eq. 10, S77 and 11), then only we would be able to calculate $i_{f-ac}[t, 2\omega]$.

$$X_2(t, \omega) = \frac{[i_{m-ac-OP}(t, 2\omega) + i_{m-ac-IP}(t, 2\omega)](1 + y^2)}{2ynFAD_O^{\frac{1}{2}}(2\omega)^{\frac{1}{2}}} \quad (11)$$

where,

$$y = 2\omega T(t, 2\omega) = \frac{i_{m-ac-OP}(t, 2\omega) + i_{m-ac-IP}(t, 2\omega)}{i_{m-ac-OP}(t, 2\omega) - i_{m-ac-IP}(t, 2\omega)} \quad (12)$$

A careful inspection of Eq. 10 and 12 reveals that $i_{m-ac-OP}(t, 2\omega)$ can never be equal to $i_{m-ac-IP}(t, 2\omega)$ for any value of y , unless and until $X_2(t, \omega) = 0$ and this condition appears only at $E(t, \omega) = E_{\frac{1}{2}}$. Therefore, y (Eq. 12) exploded to $\pm\infty$ as $E(t, \omega)$ approached to $E_{\frac{1}{2}}$. It rendered us to calculate $X_2(t, \omega)$ in the entire range of $E(t, \omega)$ by using experimentally measured values of $i_{m-ac-OP}(t, 2\omega)$ and $i_{m-ac-IP}(t, 2\omega)$. Specifically, we could be able to calculate $X_2(t, \omega)$ directly from the experimental data in both sides of $E_{\frac{1}{2}}$, but failed to do the same near to $E_{\frac{1}{2}}$ because of the nature of the function y associated with this calculation. In the one hand, we were aware of the functional form of $X_2(t, \omega)$ (Eq. 9) and on the other hand, we had the experimentally calculated values of $X_2(t, \omega)$

(Eq. 11) as a function of $E(t, \omega)$ except a range of data near to $E(t, \omega) = E_{\frac{1}{2}}$. Therefore, we adapted a hybrid (extrapolating) method to find out the most probable values of $X_2(t, \omega)$ in the entire range of $E(t, \omega)$ including $E_{\frac{1}{2}}$. We fitted the experimentally obtained $X_2(t, \omega)$ (using Eq. 12) versus $E(t, \omega)$ data with the functional form of $X_2(t, \omega)$ (Eq. 9, 13), where P, Q and S were the adjustable parameters.

$$X_2(t, \omega) = -P \sinh[Q\{E(t, \omega) - S\}] \operatorname{sech}^3[Q\{E(t, \omega) - S\}] \quad (13)$$

Then we could easily calculate $i_{f-ac}[t, 2\omega]$ of the electrochemical reaction through Eq. 8, 9 by employing computation of the fractional differentiation. Notably, $i_{f-ac}[t, 2\omega]$ is almost impossible to measure through direct experiments. The above mentioned formal developments are becoming more common in mass-transport and image processing, but their use in electroanalytical chemistry is under-explored. Therefore, this work has the ambition to introduce the use of this methodology to analytical chemists, specially involved in electrochemistry.

2 Computation and Experimental

2.1 Computational Methods and Implementations

The Riemann-Liouville-Transform (RLT) based fast semi-integration algorithm, developed in 1984, was used in several studies to simulate current from the semi-integral functions or vice-versa [50, 81, 82]. In 1999, Podlubny et al. developed a matrix approach to discrete fractional calculus following *Grunwald-Letnikov* (GL) fractional differentiation equation [83, 84]. If we consider a smooth function $f(m)$ is divided by slices of h ; then the fractional differ-integration of $f(m)$ by an arbitrary order r and lower limit l can be written as

$${}_l D_m^r = \frac{d^r f(m)}{[d(m-r)]^r} = \lim_{N \rightarrow \infty} \left[\frac{\left(\frac{m-l}{N}\right)^{-r}}{\Gamma(-r)} \sum_{q=0}^{N-1} \left\{ \frac{\Gamma(q-r)}{\Gamma(q+1)} \left(f\left(m - q\left(\frac{m-l}{N}\right)\right) \right) \right\} \right] \quad (14)$$

or

$$\frac{d^{\frac{1}{2}} f(m)}{dm^{\frac{1}{2}}} = \lim_{N \rightarrow \infty} \left[\sqrt{\frac{N}{m}} \sum_{q=0}^{N-1} \left\{ -\frac{(2j)!}{(2j-1)(2j!)^2} \left(f\left(m - \frac{qm}{N}\right) \right) \right\} \right] \quad (15)$$

where, $N = \frac{m-l}{h}$, $r = \frac{1}{2}$ and $l=0$. The Eq. 14 and 15 are known as *GL* fractional differentiation equation for the semi-derivative with lower limit to zero. For the rapid convergence of the difference quotient to the true

derivative, Eq. 15 was improved to Eq. 16, which is known as *Grunwald-Letnikov-Improved* (GLI) fractional differentiation equation. (Appendix-S8 in the *Supporting Information File*)

$$\frac{d^{\frac{1}{2}} f(m)}{dm^{\frac{1}{2}}} = \lim_{N \rightarrow \infty} \left[\sqrt{\frac{N}{m}} \sum_{q=0}^{N-1} \left\{ -\frac{(2j)!}{(2j-1)(2j!)^2} \left(f\left(m - \left(q - \frac{1}{4}\right)\left(\frac{m}{N}\right)\right) \right) \right\} \right] \quad (16)$$

This simple method provides better computational accuracy and efficiency compared to RLT based algorithm and used for image processing, edge detection and quality enhancement [85, 86]. A program was written in Python language to numerically operate the fractional differentiation. “*Differint 0.3.2*” Python package developed after 2012 was used in our program [70]. We used

GLI algorithm for the operation ${}_0 D_t^{\frac{1}{2}}$ on $X_1(t, \omega)$ and $X_2(t, \omega)$ in the floating range of t from 0 s to 1 s with $N=12000$. The computed $i_{f-ac}[t, \omega]$ and $i_{f-ac}[t, 2\omega]$ were plotted with respect to t at each $E(t, \omega)$. The peak-amplitudes of $i_{f-ac}[t, \omega]$ and $i_{f-ac}[t, 2\omega]$ at each $E(t, \omega)$ were found out through calculating root-mean-square (rms) of the evolution of the currents along t and stored for the corresponding $E(t, \omega)$. It is also interesting to mention that the term $f\left(m - \frac{qm}{N}\right)$ in Eq. 15 signifies that the derivative at m depends on the value of $f(m)$ from a point m down to its point of start at $m=0$. Therefore, the fractional differentiation reveals the non-local property of the function $f(m)$ in contrast to the integral order differentiation, which reveals only the local property of $f(m)$.

2.2 Chemicals, Instrumentations and Electrochemical Procedures

The hexaammineruthenium(III) chloride ($[\text{Ru}(\text{NH}_3)_6]\text{Cl}_3$) and potassium chloride (KCl) of analytical grades were used in this study and we did not perform any further purification of those chemicals. A solution of 5 mM ($C_o^* = 5 \times 10^{-6} \text{ mol cm}^{-3}$) $[\text{Ru}(\text{NH}_3)_6]\text{Cl}_3$ in 0.1 M KCl was freshly prepared with ultrapure Milli-Q Millipore water (18.2 MΩcm) followed by purging with high purity nitrogen for 10 min to remove the dissolved oxygen. The electrochemical experiments were performed at room temperature ($T=298 \pm 1 \text{ K}$) in a 10 mL electrochemical cell consisting of Au WE, platinum counter and an Ag/AgCl (sat. KCl) reference electrodes controlled by CHI-450B electrochemical workstation. The potentials reported in this manuscript are referred to Ag/AgCl (sat. KCl) reference electrode. The Au WE was polished using slurry of alumina powder and washed thoroughly with Milli-Q Millipore water before performing the electrochemical experiments. The gross electrochemical areas of Au WE was calculated as 0.033 cm² by using the *Randles-Sevcik* equation (Eq. 17) to the slope of the cathodic peak currents versus the square root of the scan rates (v , in the

range 0.025–0.300 V s⁻¹) in CV of 5 mM [Ru(NH₃)₆]³⁺ in 0.1 MKCl. The number of electrons transferred (*n*) and the diffusion coefficient (*D*_o) of [Ru(NH₃)₆]³⁺ in 0.1 MKCl were considered as 1 and 7.1 × 10⁻⁶ cm² s⁻¹, respectively, throughout this manuscript [87,88].

$$i_p^c = 2.69 \times 10^5 An^{\frac{3}{2}} D_o^{\frac{1}{2}} C_o^* v^{\frac{1}{2}} \quad (17)$$

$i_{m-ac-IP}(t, \omega)$, $i_{m-ac-OP}(t, \omega)$, $i_{m-ac-IP}(t, 2\omega)$ and $i_{m-ac-OP}(t, 2\omega)$ were measured by the inbuilt auto sensing Lock-in-Amplifier of CHI-450B electrochemical workstation by using its operating software with the pre-defined input parameters such as E_i , final (E_f) and step ($E_{Step} = 0.002$ V) potentials, ΔE and f of the sine wave and $t_{samp} = 1$ s (as per the design and inbuilt programme of the instrument, at each base potential the ac component of the signal was recorded for 1 s and the rms amplitude of the same was stored with respect to that base potential) and quiet time, t_q (10 s). All the reported data were stable and reproducible under the stated experimental condition. Therefore, the derived plots from the experimental data can be believed as statistically rigorous.

3 Results and Discussion

Figure 1 shows [A] $i_{m-ac-IP}(t, \omega)$, [B] $i_{m-ac-OP}(t, \omega)$ and [C] $|i_{m-ac}(t, \omega)|$ of 5 mM [Ru(NH₃)₆]³⁺ in 0.1 MKCl as a function of $E(t, \omega)$ for $\Delta E = 0.005$ V and $f =$ (i) 5 Hz, (ii) 50 Hz, (iii) 100 Hz and (iv) 500 Hz. It can be seen from Figure 1[A] that the shape of $i_{m-ac-IP}(t, \omega)$ was governed by the term $sech^2 \left[\frac{nF}{2RT} \left\{ E(t, \omega) - E_{\frac{1}{2}} \right\} \right]$ (Eq. 7, S36, S66), which became maximum at $E(t, \omega) = E_{\frac{1}{2}}$. The $E_{\frac{1}{2}}$ of [Ru(III)(NH₃)₆]³⁺/[Ru(II)(NH₃)₆]²⁺ was calculated as -0.136 ± 0.001 V and -0.134 ± 0.001 V for $f = 5$ and 50–500 Hz, respectively. The peak current of $i_{m-ac-IP}(t, \omega)$ (i.e., $i_{m-ac-IP}(t, \omega)_{Peak}$) did not vary linearly with $\sqrt{\omega}$ (Figure S1) because of the complex dependency of $i_{m-ac-IP}(t, \omega)$ on ω (Eq. S36). On the other hand, the profile of $i_{m-ac-OP}(t, \omega)$, specially near to $E_{\frac{1}{2}}$, systematically changed with increasing f (Figure 1[B]). After carefully inspecting Eq. S66, S67 and Figure 1[A, B], we speculated that non-linear $C_{DL}(t, \omega)$, which can be considered here as constant phase element due to the presence of micro-roughness on WE, might be responsible for that strange feature of $i_{m-ac-OP}(t, \omega)$. Figure 1[C] shows the trend of $|i_{m-ac}(t, \omega)|$ in the studied frequencies and it showed linear dependency with neither C_o^* nor $\sqrt{\omega}$ (Eq. 7, S36, S66–S68).

The calculated φ (degree) was found to be varied in the range 75°–15° along $E(t, \omega)$ for the studied frequencies (Figure 2[A]). It can be understood from Eq. S69, that the value of φ (degree) was dependent on the relative ratio of $\left(\frac{C_{DL}(t, \omega)}{M_1(t, \omega)} \right)$ (Figure S2). Since, $cosh^2 \left[\frac{nF}{2RT} \left\{ E(t, \omega) - E_{\frac{1}{2}} \right\} \right] \neq 0$ for any value of $E(t, \omega)$, thus the possibility for having $\varphi = 45^\circ$ raised only for $C_{DL}(t, \omega) = 0$. Further, $M_1(t, \omega)$ was always negative for all ω and $E(t, \omega)$; thus the spread of φ

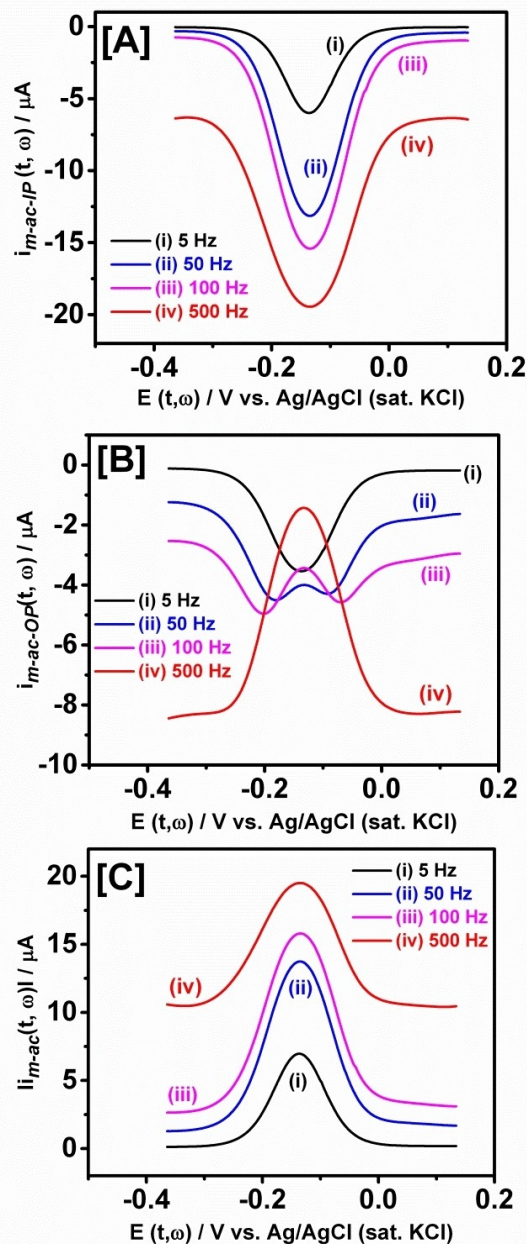


Fig. 1. [A] $i_{m-ac-IP}(t, \omega)$, [B] $i_{m-ac-OP}(t, \omega)$ and [C] $|i_{m-ac}(t, \omega)|$ of 5 mM [Ru(NH₃)₆]³⁺ in 0.1 MKCl as a function of $E(t, \omega)$ for $\Delta E = 0.005$ V and $f =$ (i) 5 Hz, (ii) 50 Hz, (iii) 100 Hz and (iv) 500 Hz.

in higher and lower to 45° suggested that $C_{DL}(t, \omega)$ changed its sign from positive to negative and then regained the positive values during the progress of $E(t, \omega)$. This assumption was confirmed from experiments as shown in Figure 2[B]. When $E(t, \omega) \gg E_{\frac{1}{2}}$, then $C_{DL}(t, \omega)$ was positive and it represented the normal electrode-electrolyte interface. As $E(t, \omega)$ approached to $E_{\frac{1}{2}}$, $C_{DL}(t, \omega)$ decreased to zero and further to negative values because, 1) the number of field oriented solvent

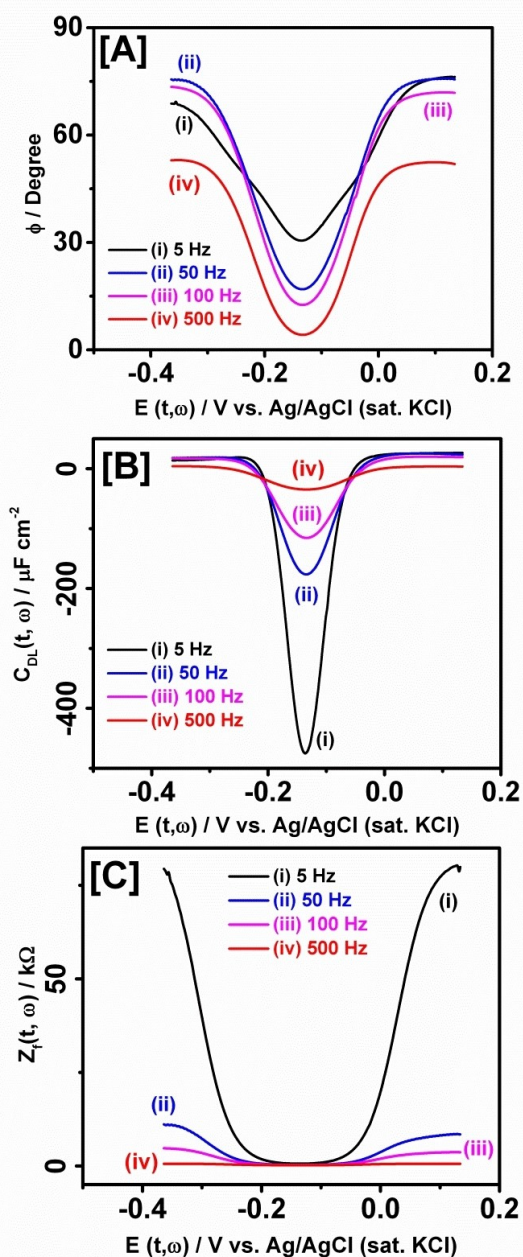


Fig. 2. [A] $\varphi(\text{degree})$, [B] $C_{DL}(t, \omega)$ and [C] $Z_f(t, \omega)$ of fundamental component of ac voltammogram of 5 mM $[\text{Ru}(\text{NH}_3)_6]^{3+}$ in 0.1 MKCl as a function of $E(t, \omega)$ for $\Delta E = 0.005$ V and $f =$ (i) 5 Hz, (ii) 50 Hz, (iii) 100 Hz and (iv) 500 Hz.

dipoles decreased in the polarized potential domain and 2) the dipoles were oriented along the direction of electric field, but redox reactions generated charge in the direction opposite to the electric field [89–91]. The φ became minimum when $\left(\frac{C_{DL}(t, \omega)}{M_1(t, \omega)}\right)$ became maximum i.e. at $E(t, \omega) = E_{\frac{1}{2}}$. As $E(t, \omega)$ went beyond $E_{\frac{1}{2}}$, the redox reaction became polarized to the surface concentration of $[\text{Ru}(\text{NH}_3)_6]^{3+}$ and $C_{DL}(t, \omega)$ again increased. When

$E(t, \omega) \ll E_{\frac{1}{2}}$, then $C_{DL}(t, \omega)$ became again positive representing the steady orientation of the charge dipoles at the interface in line to the electric field. The negative capacitance, as also experienced recently by other researchers [89–91], in the range of $E(t, \omega)$ near to $E_{\frac{1}{2}}$ could easily explain the feature of $i_{m-ac-op}(t, \omega)$ (Figure 1[B] and Eq. S67). However, it needs more fundamental independent studies and thus beyond the scope of the present manuscript.

The total faradaic impedance ($Z_f(t, \omega)$) was also dependent on $E(t, \omega)$ (Figure 2[C] and Figure S3). When $E(t, \omega) \gg E_{\frac{1}{2}}$, then $Z_f(t, \omega)$ was very high due to kinetic polarization. As $E(t, \omega)$ approached to $E_{\frac{1}{2}}$, the corresponding $Z_f(t, \omega)$ decreased and faradaic reaction took place. $Z_f(t, \omega)$ became minimum at $E(t, \omega) = E_{\frac{1}{2}}$. As $E(t, \omega)$ went beyond $E_{\frac{1}{2}}$, the redox reaction became polarized to the concentration of $[\text{Ru}(\text{NH}_3)_6]^{3+}$ and thus $Z_f(t, \omega)$ again increased. $Z_f(t, \omega)$ was basically a linear combination of the charge-transfer resistance (R_{CT}) and Warburg impedance (W). At $E(t, \omega) > E_{\frac{1}{2}}$, R_{CT} dominated, while W dominated at $E(t, \omega) < E_{\frac{1}{2}}$. Further, $Z_f(t, \omega)$ increased with decreasing f , because the probability of the electrochemical charge transfer reaction increased at lower frequencies.

The peak amplitude ($X_1(t, \omega)$) of the fundamental component ($m_1(t, \omega)$) of ac voltammogram (Eq. S35) as a function of $E(t, \omega)$ is shown in Figure 3[A]. It can be seen that the shape of $X_1(t, \omega)$ was governed by the term $\text{sech}^2\left[\frac{nF}{2RT}\left\{E(t, \omega) - E_{\frac{1}{2}}\right\}\right]$ and it was dependent on ω in such a way that as ω increased, the peak height of $X_1(t, \omega)$ decreased. Figure 3[B](a) shows the sinusoidal progress of $m_1(t, \omega)$ with respect to t for $E(t, \omega) = -0.136$ V and $f = 5$ Hz. Upon operating ${}_0D_t^{\frac{1}{2}}$ on $m_1(t, \omega)$ we computationally derived the corresponding faradaic fundamental alternating current ($i_{f-ac}[t, \omega]$) (Figure 3[B](b)). It can be seen that the derived sinusoidal $i_{f-ac}[t, \omega]$ was ahead in a phase by $45.3 \pm 0.1^\circ$ (theoretically it should be 45° (Eq. 6, S35)) compared to $m_1(t, \omega)$. It confirmed that our computation method was satisfactorily meeting the goal. Figure 3[C] shows the $i_{f-ac}[t, \omega]$ as a function of $E(t, \omega)$. By comparing Figure 1[C] with Figure 3[C], one can say that the $i_{f-ac}[t, \omega]$ was relatively higher to the corresponding $|i_{m-ac}(t, \omega)|$ for any $E(t, \omega)$. It ensures that the current signal was diminished to an extent by the action of the negative double layer capacitances. We considered $D_{[\text{Ru}(\text{NH}_3)_6]^{3+}}$ and $D_{[\text{Ru}(\text{NH}_3)_6]^{2+}}$ as 7.1×10^{-6} and 7.8×10^{-6} $\text{cm}^2 \text{s}^{-1}$, respectively, and we calculated ξ as 0.954 [81, 82].

By using Eq. S16 and S35, we could compute the % variation in $C_O(0, t, \omega)$ and $C_R(0, t, \omega)$ relative to C_O^* for fundamental component of ac voltammetry (Figure 3[D]). Notably, here we did not consider the variation of the surface concentrations for the linear scan component. The

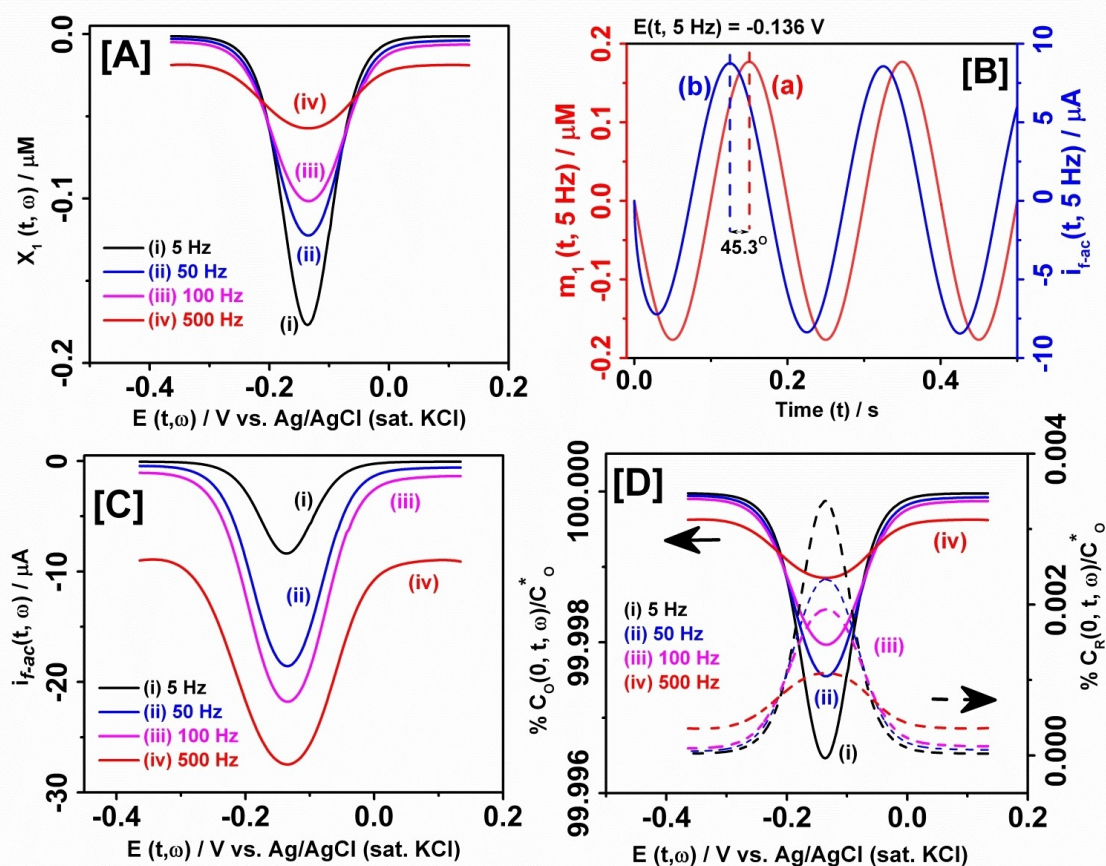


Fig. 3. [A] Peak amplitude ($X_1(t, \omega)$) of the fundamental component ($m_1(t, \omega)$) of ac voltammogram (Eq. S35) as a function of $E(t, \omega)$ for $\Delta E = 0.005$ V and $f = (i)$ 5 Hz, (ii) 50 Hz, (iii) 100 Hz and (iv) 500 Hz. [B] The sinusoidal progress of (a) $m_1(t, \omega)$ and (b) faradaic fundamental alternating current ($i_{f-ac}[t, \omega]$) with respect to t for $f = 5$ Hz and $E(t, \omega) = -0.136$ V. [C] $i_{f-ac}[t, \omega]$ and [D] $\% \frac{C_O(0, t, \omega)}{C_O^*}$ and $\% \frac{C_R(0, t, \omega)}{C_O^*}$ of 5 mM $[\text{Ru}(\text{NH}_3)_6]^{3+}$ in 0.1 M KCl as a function of $E(t, \omega)$ for $\Delta E = 0.005$ V and $f = (i)$ 5 Hz, (ii) 50 Hz, (iii) 100 Hz and (iv) 500 Hz.

overall variation in $C_O(0, t, \omega)$ and $C_R(0, t, \omega)$ did not exceed $\pm 0.004\%$ relative to C_O^* during the sine potential perturbations. The small change in $C_O(0, t, \omega)$ and $C_R(0, t, \omega)$ at $E(t, \omega) > E_{1/2}$ and $E(t, \omega) < E_{1/2}$ was attributed to the kinetic and concentration polarizations, respectively. The maximum change in the surface concentrations was observed at $E(t, \omega) \sim E_{1/2}$ and the extent of changes decreased as the duration of potential perturbation decreased (i.e. frequency of the perturbation increased).

Figure 4 shows [A, D] $i_{m-ac-IP}(t, 2\omega)$, [B, E] $i_{m-ac-OP}(t, 2\omega)$ and [C, F] $|i_{m-ac}(t, 2\omega)|$ of 5 mM $[\text{Ru}(\text{NH}_3)_6]^{3+}$ in 0.1 M KCl as a function of $E(t, \omega)$ for [A, B, C] $f = 50$ Hz and $\Delta E = (i)$ 0.005 V, (ii) 0.025 V, (iii) 0.050 V, (iv) 0.075 V, (v) 0.100 V, (vi) 0.125 V and for [D, E, F] $\Delta E = 0.125$ V and $f = (i)$ 25 Hz, (ii) 50 Hz, (iii) 75 Hz and (iv) 100 Hz. As expected from Eq. 10, S76, $i_{m-ac-IP}(t, 2\omega)$, $i_{m-ac-OP}(t, 2\omega)$ and $|i_{m-ac}(t, 2\omega)|$ all significantly increased with increasing ΔE . The shape of the measured harmonic currents evolved with increasing ΔE . In the contrast, only the shape of $i_{m-ac-IP}(t, 2\omega)$ evolved

with increasing f , insignificant changes were observed in $i_{m-ac-OP}(t, 2\omega)$ and $|i_{m-ac}(t, 2\omega)|$ at different f in the range 25–100 Hz. As discussed in the Section 1.2, $i_{m-ac-IP}(t, 2\omega)$, $i_{m-ac-OP}(t, 2\omega)$ and $|i_{m-ac}(t, 2\omega)|$ became zero at $E(t, \omega) = E_{1/2}$. Therefore, SHac voltammetry was indeed a good method to experimentally find the $E_{1/2}$ of an electrochemically reversible reaction.

Figure 5 [A, B] show that $\varphi_{SH}(\text{degree})$ of $i_{m-ac}(t, 2\omega)$ with respect to $E(t, \omega)$ changed by $\sim 180^\circ$ at $E(t, \omega) = E_{1/2}$ irrespective of the value of [A] ΔE and [B] f . Thus it could represent the point of discontinuity (or singularity) at $E(t, \omega) \approx E_{1/2}$ and it was indeed another signature of $E_{1/2}$, which could be used to identify corresponding $E_{1/2}$ s in a mixed redox system. As we discussed in the Section 1.2 that the singularity issue near to $E_{1/2}$ rendered us to calculate $X_2(t, \omega)$ directly from $i_{m-ac-IP}(t, 2\omega)$ and $i_{m-ac-OP}(t, 2\omega)$ in the entire range of $E(t, \omega)$. We adopted a

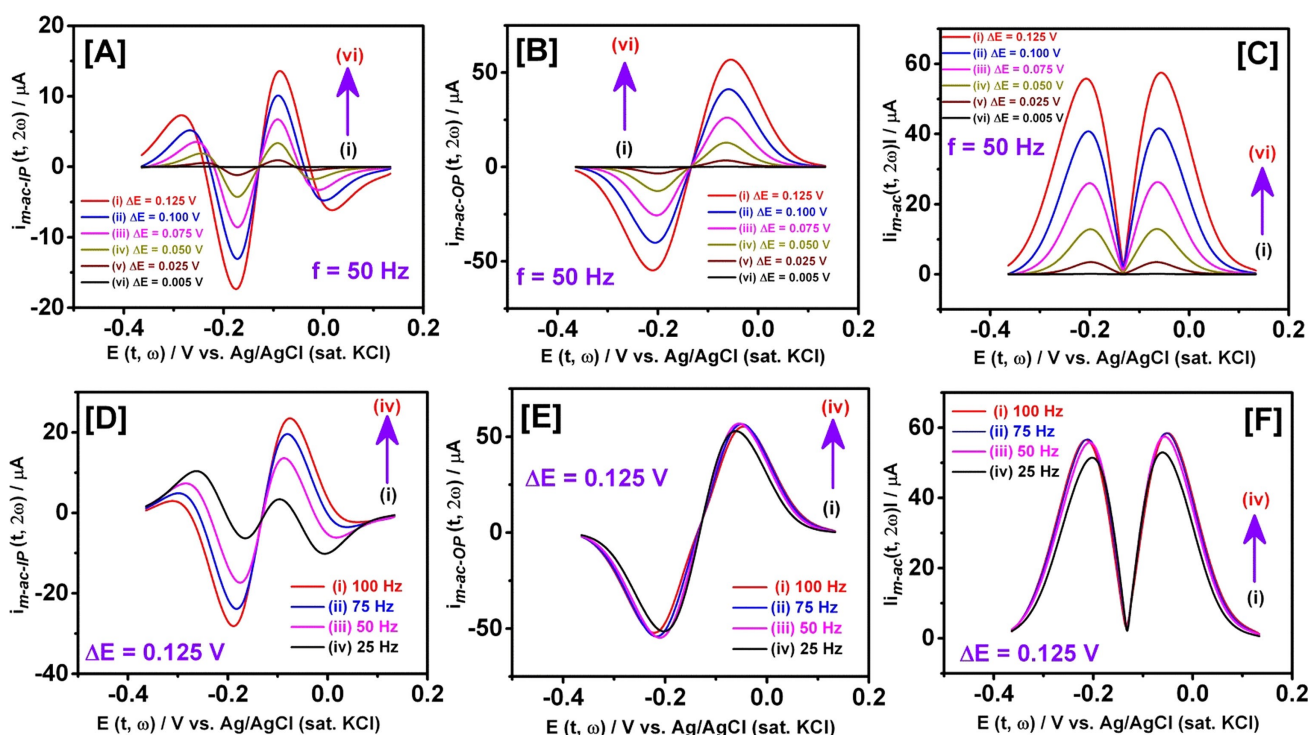


Fig. 4. [A, D] $i_{m-ac-IP}(t, 2\omega)$, [B, E] $i_{m-ac-OP}(t, 2\omega)$ and [C, F] $|i_{m-ac}(t, 2\omega)|$ of 5 mM $[\text{Ru}(\text{NH}_3)_6]^{3+}$ in 0.1 M KCl as a function of $E(t, \omega)$ for [A, B, C] $f = 50$ Hz and $\Delta E =$ (i) 0.005 V, (ii) 0.025 V, (iii) 0.050 V, (iv) 0.075 V, (v) 0.100 V, (vi) 0.125 V and for [D, E, F] $\Delta E = 0.125$ V and $f =$ (i) 25 Hz, (ii) 50 Hz, (iii) 75 Hz and (iv) 100 Hz.

hybrid-experimental-computation method to calculate $X_2(t, \omega)$.

Figure 5[C] shows the measured (blue dots) and computed (red line) $X_2(t, \omega)$ at $\Delta E = 0.125$ V and $f = 50$ Hz. We have listed all the fitted parameters in Table S1 to confirm the suitability of the hybrid-experimental-computation method for this purpose. The deviations of the fitted parameters with the theoretically expected values might be many folds including the interference of ΔE and f into the overall response. Figure S3 shows $X_2(t, \omega)$ with respect to $E(t, \omega)$ at different [A] ΔE and [B] f . $X_2(t, \omega)$ increased with increasing ΔE , but f had almost no influence on $X_2(t, \omega)$. For all ΔE and f , $X_2(t, \omega)$ became zero at $E(t, \omega) = E_{\frac{1}{2}}$ and φ_{SH} of $X_2(t, \omega)$ at peak

positions i.e.; at $[E(t, \omega) - E_{\frac{1}{2}}] = \pm 1.317 \frac{RT}{nF}$ differed by 180° . Evidently, similar to $E_{\frac{1}{2}}$, the peak position was dependent on ΔE and f because of the dependency of $E(t, \omega)$ on ΔE and f . Upon computationally operating ${}_0D_t^{\frac{1}{2}}$ on $m_2(t, \omega)$ (Eq. S52), we numerically calculated $i_{f-ac}(t, 2\omega)$. Peaks of $X_2(t, \omega)$ for $\Delta E = 0.125$ V and $f = 50$ Hz were observed at -0.074 V and -0.184 V. Figure 5 [D] shows $i_{f-ac}(t, 2\omega)$ as a function of t at $E(t, \omega) =$ (i) -0.074 V and (ii) -0.184 V for $\Delta E = 0.125$ V and $f = 50$ Hz. The phase difference of $i_{f-ac}(t, 2\omega)$ at the peak potentials was calculated as $180.2 \pm 0.1^\circ$ (theoretically it should be 180°) at any t and it again proved the suitability

of our computational method of analysis in the objective of this article. Figure 5 shows $|i_{f-ac}(t, 2\omega)|$ of 5 mM $[\text{Ru}(\text{NH}_3)_6]^{3+}$ in 0.1 M KCl as a function of $E(t, \omega)$ for [E] $\Delta E =$ (i) 0.005, (ii) 0.025, (iii) 0.050, (iv) 0.075, (v) 0.100 and (vi) 0.125 V and [F] $f =$ (i) 25, (ii) 50, (iii) 75 and (iv) 100 Hz. Comparing Figure 4[C, F] with Figure 5[E, F], one can say that $|i_{f-ac}(t, \omega)|$ was relatively higher to corresponding $|i_{m-ac}(t, \omega)|$ for any $E(t, \omega)$.

4 Conclusion

We have successfully used the theory of general fractional-order calculus to derive the working equations of ac and SHac voltammetry considering the non-local information of the surface concentrations of the analyte. We also explored the possible ways to extract some of the useful information about electrode-electrolyte interface in the potential range of analysis for an electrochemically reversible reaction. The simple potentiostat having inbuilt lock-in-amplifier was sufficient for this purpose. We were successful to numerically compute the true faradaic fundamental and second harmonic components of ac voltammogram, for an electrochemically reversible reaction by using our developed computational code with fractional calculus. That information was almost impossible or very difficult to measure through performing only experiments. Authors believe that the above discussed methodology is certainly explorative beyond the second harmonic and electrochemically reversible reaction.

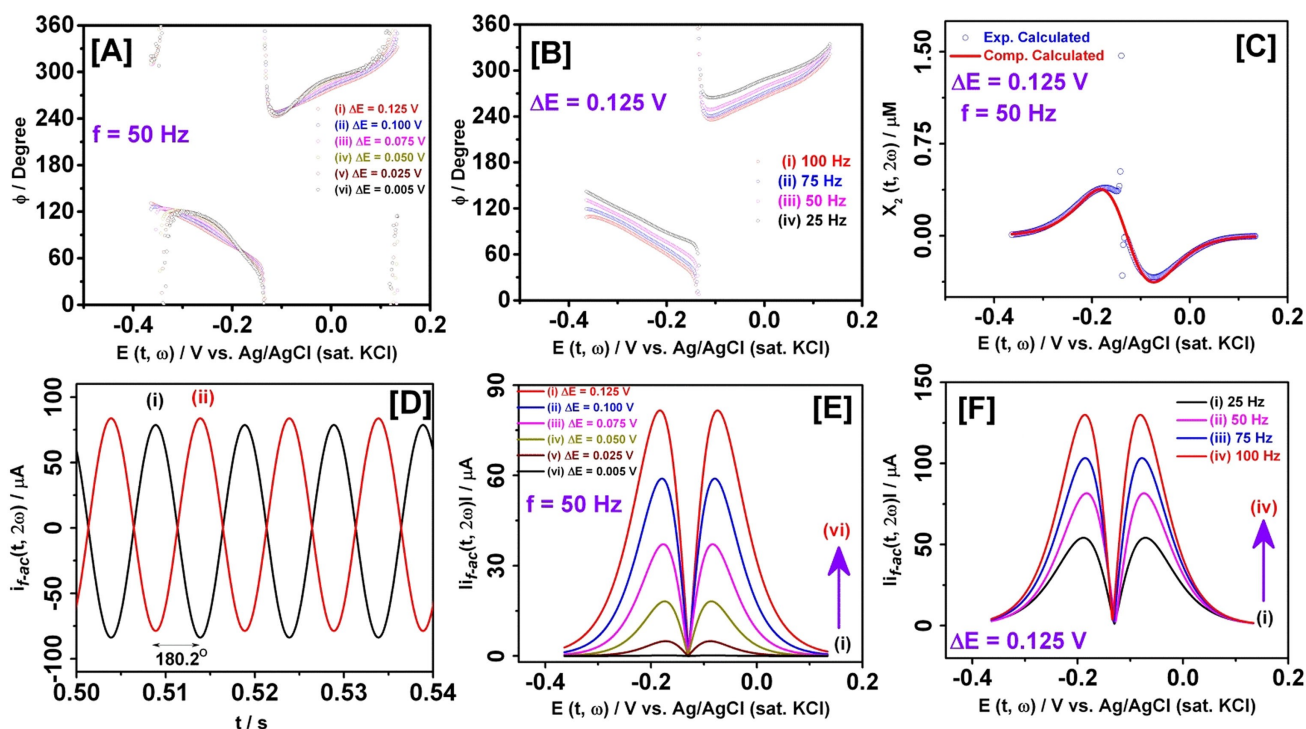


Fig. 5. (degree) of $i_{m-ac}(t, 2\omega)$ with respect to $E(t, \omega)$ for [A] $f=50$ Hz and $\Delta E=(i)$ 0.125 V, (ii) 0.100 V, (iii) 0.075 V, (iv) 0.050 V, (v) 0.025 V, (vi) 0.005 V and [B] $\Delta E=0.125$ V and $f=(i)$ 100 Hz, (ii) 75 Hz, (iii) 50 Hz, (iv) 25 Hz. [C] The measured (blue dots) and computed (red line) $X_2(t, 2\omega)$ at $\Delta E=0.125$ V and $f=50$ Hz, representing the point of discontinuity (or singularity) at $E(t, \omega) \approx E_1$. [D] $i_{f-ac}(t, 2\omega)$ as a function of t at $E(t, \omega)=(i)$ -0.074 V and (ii) -0.184 V for $\Delta E=0.125$ V and $f=50$ Hz. The computed $|i_{f-ac}(t, 2\omega)|$ of 5 mM $[\text{Ru}(\text{NH}_3)_6]^{3+}$ in 0.1 MKCl as a function of $E(t, \omega)$ for [E] $f=50$ Hz and $\Delta E=(i)$ 0.005 V, (ii) 0.025 V, (iii) 0.050 V, (iv) 0.075 V, (v) 0.100 V, (vi) 0.125 V and [F] $\Delta E=0.125$ V and $f=(i)$ 25 Hz, (ii) 50 Hz, (iii) 75 Hz, (iv) 100 Hz.

List of Abbreviations Used in the Main Article and Supporting Information File

ac voltammetry	Alternating current voltammetry
CV	Cyclic voltammetry
dc	Direct current
EIS	Electrochemical impedance spectroscopy
Fac voltammetry	Fundamental component of alternating current voltammetry
GLI	Grunwald-Letnikov-Improved fractional differentiation equation
IP	In-phase component of current
OP	Out-of-phase component of current
RL	Reimann-Liouville
rms	Root-mean-square
SHac voltammetry	Second harmonic component of alternating current voltammetry
WE	Working electrode

List of Symbols used in the Main Article and Supporting Information

$\bar{C}_O(x, f, \omega)$	Laplace transformed form of $C_O(x, t, \omega)$
$\bar{C}_R(x, f, \omega)$	Laplace transformed form of $C_R(x, t, \omega)$

$\frac{d^{\frac{1}{2}}f(m)}{dm^{\frac{1}{2}}}$	Half-order differentiation of $f(m)$ with respect to m
$ i_{m-ac}[t, 2\omega] $	Measured amplitude of the second harmonic component of ac response
$ i_{m-ac}[t, \omega] $	Measured amplitude of the fundamental component of ac response
$\frac{\delta^2}{\delta x^2}$	Classical second-order differential operator with respect to x
${}_0D_t^{\frac{1}{2}}$	Fractional differentiation operator
\mathcal{L}^{-1}	Inverse of Laplace-transformation operator (\mathcal{L})
$C_{DL}(t, 2\omega)$	Double layer capacitance generated with second-harmonic component of ac response; The derived values of the capacitance from the experimental data may not represent the ideal capacitor behavior due to the micro-roughness of WE and can be considered as constant phase element.
$C_{DL}(t, \omega)$	Double layer capacitance generated with fundamental component of ac response; The derived values of the capacitance from the experimental data may not represent the ideal capacitor behavior due to the micro-roughness of WE and can be considered as constant phase element.

$C_O(x, t, \omega)$	Concentration of O at distance x, time t and applied angular frequency ω	*	Convolution operator
C_O^*	Bulk concentration of O in solution	Δ	$= \frac{nF}{RT} (E_i - E_{1/2}^0)$; A constant for any specified experimental condition
$C_R(x, t, \omega)$	Concentration of R at distance x, time t and applied angular frequency ω	A	Area of WE
D_O	Diffusion coefficient of O	a	Starting point of variable m in Reimann-Liouville fractional integral operator
D_R	Diffusion coefficient of R	Au	Gold (macro-disk) working electrode
$E_{1/2}$	Half-wave potential	C_{DL}	Double layer capacitance
E_0'	Formal redox potential	d	$= \frac{nF}{RT} (vt + \Delta E \sin \omega t)$
$E_b(t, \omega)$	Base potential of the ac signal	f	Linear frequency
E_f	Final potential of the applied signal	F	Faraday's constant
E_i	Initial potential of the applied signal	f(m)	A smooth function of arbitrary variable m
E_{step}	Step potential of the applied signal	h	Number of slices in of intervals in the dependent variable
$J_{d=0,t}$	Concentration gradient of the analyte at the electrode surface	j	$\sqrt{-1}$
$M_1(t, \omega)$	Amplitude of the $i_{f-ac}[t, \omega]$	l	Lower limit of the variable m
R_u	Uncompensated cell resistance	m	Arbitrary variable in mathematical operations
$X_1(t, \omega)$	Amplitude of $m_1(t, \omega)$	N	Total number of intervals
$X_2(t, \omega)$	Amplitude of $m_2(t, \omega)$	n	Number of electrons involved in the redox reaction
$X_3(t, \omega)$	An intermediate parameter in derivation	O	Oxidized form of the redox couple
$Z_f(t, \omega)$	Faradaic impedance	P, Q, S	Adjustable parameters of fitting (in Origin Software) the experimental data with theoretically derived expressions
${}_a I_x^\alpha$	Reimann-Liouville fractional integral operator	q	Arbitrary index in mathematical operation
$i_c(t)$	Capacitive current	R	Reduced form of the redox couple
$i_{c-ac}[t, \omega]$	Capacitive component ac response	r	Arbitrary order of differ-integration
$i_{dc}(t, \omega)$	Current response without influence of ω	R	Universal gas constant
$i_f(t)$	Faradaic current	R_{CT}	Charge transfer resistance
$i_{f-ac}[t, 2\omega]$	Computed second-harmonic component of true faradaic ac response	t	Time
$i_{f-ac}[t, \omega]$	Computed fundamental component of true faradaic ac response	T	Temperature in the absolute (Kelvin) scale
$i_{m-ac}[t, 2\omega]$	Measured second-harmonic component of ac response	t_q	Quiet time
$i_{m-ac}[t, \omega]$	Measured fundamental component of ac response	t_{smp}	Time required for sampling current by lock-in-amplifier of the potentiostat
$i_{m-ac-IP}(t, 2\omega)$	Measured in-phase second-harmonic component of ac response	W	Warburg impedance
$i_{m-ac-IP}(t, \omega)$	Measured in-phase fundamental component of ac response	σ_w	Warburg coefficient
$i_{m-ac-OP}(t, 2\omega)$	Measured out-of-phase second-harmonic component of ac response	ω	Angular frequency
$i_{m-ac-OP}(t, \omega)$	Measured out-of-phase fundamental component of ac response	$E(t, \omega)$	Applied ac potential
i_p^c	Cathodic peak current of CV	$E(t)$	Applied potential
k_0	Standard heterogeneous electron transfer rate constant	$T(t, 2\omega)$	Time constant of the second-harmonic component of ac voltammetry
$m_0(t, \omega)$	Semi-integral representing dc component of $m(t, \omega)$	$f(m)$	Arbitrary function of variable m
$m_1(t, \omega)$	Semi-integral representing fundamental ac component of $m(t, \omega)$	$i(t)$	Measured current
$m_2(t, \omega)$	Semi-integral representing second-harmonic component of $m(t, \omega)$	$i(t, \omega)$	Measured ac response
α_c	Electron transfer coefficient	$m(t, \omega)$	Total semi-integral
$\frac{\delta}{\delta t}$	Classical first order differential operator with respect to t	$p(t, 2\omega)$	In-situ potential drop across the electrochemical cell at second harmonic
$\varphi_{SH}(degree)$	Phase shift between the $E(t, \omega)$ and $i_{m-ac}[t, 2\omega]$ in four-quadrants	$p(t, \omega)$	Sine potential perturbation in ac voltammetry
		u	An arbitrary variable for mathematical operations
		x	Distance (perpendicular to the electrode) from the electrode surface
		y	$= 2\omega T(t, 2\omega)$
		f	Laplace transformed form of t
		$\Gamma(\alpha)$	Gamma function of α

ΔE	Amplitude of sine perturbation
α	Order of Reimann-Liouville fractional integral operator
$\theta(t, \omega)$	A dimensionless function of potential
ν	Scan rate of the potential signal
ξ	Dimensionless variable involving D_O and D_R
$\varphi(\text{degree})$	Phase shift between the $E(t, \omega)$ and $i_{m-ac}(t, \omega)$ in four-quadrants
$\chi(t, \omega)$	A dimensionless current function used in the derivation
$\psi(t, \omega)$	Dimensionless ac response
$\psi(f, \omega)$	Laplace transformed form of $\psi(t, \omega)$

Special Note

The computer program code related to this study can be shared on request to the corresponding author through email. The user will be responsible for its acknowledgement and further dissemination.

Acknowledgements

Dr. Saurav K. Guin sincerely acknowledges the expert advice and guidance received from Prof. Alan M. Bond, School of Chemistry, Monash University, Australia in the subject and preparation of the revised manuscript. He also acknowledges the suggestions received from with Dr. Swapan Kumar Ghosh, Dr. Alok Samanta, TCS, BARC, Dr. Dhanadeep Datta, RCD, BARC. Dr. Saurav K. Guin and Arvind S. Amolikar extend their gratitude to Dr. S. Kannan, Dr. (Mrs.) Renu Agarwal, Dr. Satyajeet Chaudhury of FCD, BARC for their kind interest and extended support in this research work.

Conflict of Interest

The authors declare no conflict of interest.

References

- W. L. Underkofler, I. Shain, *Anal. Chem.* **1965**, *37*, 218–222.
- D. E. Smith, in *Electroanal. Chem. V. 1* (Ed.: Allen J. Bard), Marcel Dekker, New York, **1966**, pp. 1–155.
- T. G. McCord, D. E. Smith, *Anal. Chem.* **1968**, *40*, 289–304.
- T. G. McCord, D. E. Smith, *Anal. Chem.* **1968**, *40*, 1959–1966.
- D. E. Glover, D. E. Smith, *Anal. Chem.* **1971**, *43*, 775–779.
- S. C. Creason, J. W. Hayes, D. E. Smith, *J. Electroanal. Chem. Interfacial Electrochem.* **1973**, *47*, 9–46.
- H. Blustein, A. M. Bond, A. Norris, *Anal. Chem.* **1976**, *48*, 1975–1979.
- A. M. Bond, R. J. O'Halloran, I. Ruzic, D. E. Smith, *Anal. Chem.* **1976**, *48*, 872–883.
- R. J. Schwall, A. M. Bond, R. J. Loyd, J. G. Larsen, D. E. Smith, *Anal. Chem.* **1977**, *49*, 1797–1805.
- C. I. Mooring, H. L. Kies, *J. Electroanal. Chem. Interfacial Electrochem.* **1977**, *78*, 219–227.
- A. M. Bond, R. J. O'Halloran, I. Ruzic, D. E. Smith, *Anal. Chem.* **1978**, *50*, 216–223.
- A. M. Bond, R. J. O'Halloran, I. Ruzic, D. E. Smith, *J. Electroanal. Chem. Interfacial Electrochem.* **1978**, *90*, 381–388.
- J. E. Anderson, A. M. Bond, *Anal. Chem.* **1981**, *53*, 1394–1398.
- J. Házia, D. M. Elton, W. A. Czerwinski, J. Schiewe, V. A. Vicente-Beckett, A. M. Bond, *J. Electroanal. Chem.* **1997**, *437*, 1–15.
- D. J. Gavaghan, A. M. Bond, *J. Electroanal. Chem.* **2000**, *480*, 133–149.
- G. P. Morris, A. N. Simonov, E. A. Mashkina, R. Bordas, K. Gillow, R. E. Baker, D. J. Gavaghan, A. M. Bond, *Anal. Chem.* **2013**, *85*, 11780–11787.
- A. M. Bond, D. Elton, S.-X. Guo, G. F. Kennedy, E. Mashkina, A. N. Simonov, J. Zhang, *Electrochem. Commun.* **2015**, *57*, 78–83.
- G. F. Kennedy, A. M. Bond, A. N. Simonov, *Curr. Opin. Electrochem.* **2017**, *1*, 140–147.
- Y. Zhang, A. N. Simonov, J. Zhang, A. M. Bond, *Curr. Opin. Electrochem.* **2018**, *10*, 72–81.
- D. J. Gavaghan, D. Elton, K. B. Oldham, A. M. Bond, *J. Electroanal. Chem.* **2001**, *512*, 1–15.
- D. J. Gavaghan, D. Elton, A. M. Bond, *J. Electroanal. Chem.* **2001**, *513*, 73–86.
- D. J. Gavaghan, J. C. Myland, K. B. Oldham, *J. Electroanal. Chem.* **2001**, *516*, 2–9.
- K. B. Oldham, D. J. Gavaghan, A. M. Bond, *J. Phys. Chem. B* **2002**, *106*, 152–157.
- S.-X. Guo, J. Zhang, D. M. Elton, A. M. Bond, *Anal. Chem.* **2004**, *76*, 166–177.
- S.-X. Guo, A. M. Bond, J. Zhang, *Rev. Polarography* **2015**, *61*, 21–32.
- C. P. Andrieux, P. Hapiot, J. Pinson, J. M. Saveant, *J. Am. Chem. Soc.* **1993**, *115*, 7783–7788.
- S. E. Creager, T. T. Wooster, *Anal. Chem.* **1998**, *70*, 4257–4263.
- D. A. Brevnov, H. O. Finklea, *J. Electroanal. Chem.* **2000**, *488*, 133–139.
- J. Zhang, S.-X. Guo, A. M. Bond, F. Marken, *Anal. Chem.* **2004**, *76*, 3619–3629.
- A. M. Bond, N. W. Duffy, S.-X. Guo, J. Zhang, D. Elton, *Anal. Chem.* **2005**, *77*, 186A–195A.
- A. J. Lucio, S. K. Shaw, J. Zhang, A. M. Bond, *J. Phys. Chem. C* **2017**, *121*, 12136–12147.
- H. Adamson, A. M. Bond, A. Parkin, *Chem. Commun.* **2017**, *53*, 9519–9533.
- S.-Y. Tan, R. A. Lazenby, K. Bano, J. Zhang, A. M. Bond, J. V. Macpherson, P. R. Unwin, *Phys. Chem. Chem. Phys.* **2017**, *19*, 8726–8734.
- C. Sun, F. Li, H. An, Z. Li, A. M. Bond, J. Zhang, *Electrochim. Acta* **2018**, *269*, 733–741.
- J. Li, G. F. Kennedy, A. M. Bond, J. Zhang, *J. Phys. Chem. C* **2018**, *122*, 9009–9014.
- C. G. Bell, C. A. Anastassiou, D. O'Hare, K. H. Parker, J. H. Siggers, *Electrochim. Acta* **2011**, *56*, 6131–6141.
- C. G. Bell, C. A. Anastassiou, D. O'Hare, K. H. Parker, J. H. Siggers, *Electrochim. Acta* **2011**, *56*, 7569–7579.
- C. G. Bell, C. A. Anastassiou, D. O'Hare, K. H. Parker, J. H. Siggers, *Electrochim. Acta* **2011**, *56*, 8492–8508.
- C. L. Bentley, A. M. Bond, A. F. Hollenkamp, P. J. Mahon, J. Zhang, *Anal. Chem.* **2014**, *86*, 2073–2081.
- K. B. Oldham, J. Spanier, *J. Electroanal. Chem. Interfacial Electrochem.* **1970**, *26*, 331–341.

- [41] K. B. Oldham, J. Spanier, *J. Math. Anal. Appl.* **1972**, *39*, 655–669.
- [42] M. Grenness, K. B. Oldham, *Anal. Chem.* **1972**, *44*, 1121–1129.
- [43] K. B. Oldham, *J. Electroanal. Chem. Interfacial Electrochem.* **1973**, *41*, 351–358.
- [44] K. B. Oldham, J. Spanier, *The Fractional Calculus Theory and Applications of Differentiation and Integration to Arbitrary Order*, Academic Press, New York, **1974**.
- [45] P. J. Mahon, K. B. Oldham, *J. Electroanal. Chem.* **1998**, *445*, 179–195.
- [46] S. O. Engblom, J. C. Myland, K. B. Oldham, *J. Electroanal. Chem.* **2000**, *480*, 120–132.
- [47] S. O. Engblom, J. C. Myland, K. B. Oldham, A. L. Taylor, *Electroanalysis* **2001**, *13*, 626–630.
- [48] K. B. Oldham, *Adv. Eng. Soft.* **2010**, *41*, 9–12.
- [49] K. B. Oldham, J. C. Myland, *Electrochim. Acta* **2011**, *56*, 10612–10625.
- [50] K. B. Oldham, J. C. Myland, A. M. Bond, E. A. Mashkina, A. N. Simonov, *J. Electroanal. Chem.* **2014**, *719*, 113–121.
- [51] A. M. P. Sakita, R. D. Noce, C. S. Fugivara, A. V. Benedetti, *Anal. Chem.* **2017**, *89*, 8296–8303.
- [52] P. J. Mahon, K. B. Oldham, *ChemElectroChem* **2018**, *5*, 839–848.
- [53] S. A. David, J. L. Linares, E. M. J. A. Pallone, *Rev. Bras. Ensino Fis.* **2011**, *33*, 4302–4302.
- [54] J. A. T. Machado, A. M. S. F. Galhano, J. J. Trujillo, *Scientometrics* **2014**, *98*, 577–582.
- [55] S. Das, *Functional Fractional Calculus*, Springer-Verlag Berlin Heidelberg, Heidelberg, **2011**.
- [56] J. Sabatier, M. Cugnet, S. Laruelle, S. Grugeon, B. Sahut, A. Oustaloup, J. M. Tarascon, *Commun. Nonlinear Sci. Numer. Simulat.* **2010**, *15*, 1308–1317.
- [57] T. J. Freeborn, B. Maundy, A. S. Elwakil, *Mater Renew Sustain Energy* **2015**, *4*, 9.
- [58] J. F. Gómez-Aguilar, J. E. Escalante-Martínez, C. Calderón-Ramón, L. J. Morales-Mendoza, M. Benavidez-Cruz, M. Gonzalez-Lee, *Adv. Math. Phys.* **2016**, 9720181.
- [59] C. Zou, L. Zhang, X. Hu, Z. Wang, T. Wik, M. Pecht, *J. Power Sources* **2018**, *390*, 286–296.
- [60] A. Allagui, T. J. Freeborn, A. S. Elwakil, M. E. Fouda, B. J. Maundy, A. G. Radwan, Z. Said, M. A. Abdelkareem, *J. Power Sources* **2018**, *400*, 457–467.
- [61] Q. Zhang, Y. Li, Y. Shang, B. Duan, N. Cui, C. Zhang, *Electronics* **2019**, *8*, 394.
- [62] J. I. Hidalgo-Reyes, J. F. Gómez-Aguilar, R. F. Escobar-Jiménez, V. M. Alvarado-Martínez, M. G. López-López, *Microelectron. J.* **2019**, *85*, 109–128.
- [63] V. Mirčeski, Ž. Tomovski, *J. Phys. Chem. B* **2009**, *113*, 2794–2799.
- [64] M. Grdeň, *J. Solid State Electrochem.* **2017**, *21*, 1045–1058.
- [65] J. C. Imbeaux, J. M. Savéant, *J. Electroanal. Chem. Interfacial Electrochem.* **1973**, *44*, 169–187.
- [66] L. Nadjo, J. M. Savéant, D. Tessier, *J. Electroanal. Chem. Interfacial Electrochem.* **1974**, *52*, 403–412.
- [67] J. M. Savéant, D. Tessier, *J. Electroanal. Chem. Interfacial Electrochem.* **1975**, *61*, 251–263.
- [68] J. M. Savéant, D. Tessier, *J. Electroanal. Chem. Interfacial Electrochem.* **1975**, *65*, 57–66.
- [69] Y. Uchida, E. Kätelhön, R. G. Compton, *J. Electroanal. Chem.* **2017**, *801*, 381–387.
- [70] D. Baleanu, K. Diethelm, E. Scalas, J. J. Trujillo, *Fractional Calculus: Models and Numerical Methods*, World Scientific Pub Co Inc., **2012**.
- [71] C.-M. Chi, F. Gao, *J. Softw.* **2013**, *8*, 572–578.
- [72] Z. Li, L. Liu, S. Dehghan, Y. Q. Chen, D. Xue, *Int. J. Control* **2017**, *90*, 1165–1181.
- [73] R. Garrappa, *Mathematics* **2018**, *6*, 16.
- [74] K. B. Oldham, J. C. Myland, A. M. Bond, *Electrochemical Science and Technology: Fundamentals and Applications*, **2011**, John Wiley & Sons, Ltd., ISBN: 9780470710845.
- [75] P. He, L. R. Faulkner, *Anal. Chem.* **1986**, *58*, 517–523.
- [76] P. He, X. Chen, *Anal. Chem.* **1990**, *62*, 1331–1338.
- [77] K. B. Oldham, *J. Electroanal. Chem. Interfacial Electrochem.* **1979**, *105*, 373–375.
- [78] J. C. Myland, K. B. Oldham, *J. Electroanal. Chem. Interfacial Electrochem.* **1983**, *153*, 43–54.
- [79] K. B. Oldham, *J. Electroanal. Chem.* **1997**, *430*, 1–14.
- [80] K. B. Oldham, J. Myland, J. Spanier, *An Atlas of Functions with Equator, the Atlas Function Calculator*, Springer, New York, **2009**.
- [81] T. Pajkossy, L. Nyikos, *J. Electroanal. Chem.* **1984**, *179*, 65–69.
- [82] T. Pajkossy, *Electrochim. Acta* **2019**, *308*, 410–417.
- [83] I. Podlubny, *Fractional Differential Equations: An Introduction to Fractional Derivatives, Fractional Differential Equations, Some Methods of Their Solution and Some of Their Applications*. Academic Press, San Diego-Boston-New York-London-Tokyo-Toronto, **1999**, 368 pages. ISBN 0125588402.
- [84] I. Podlubny, *Int. J. Theor. Appl.* **2000**, *3*, 359–386.
- [85] Y. Khan, Q. Wu, N. Faraz, A. Yildirim, M. Madani, *Appl. Math. Lett.* **2012**, *25*, 1340–1346.
- [86] H. Jalalinejad, A. Tavakoli, F. Zarmehi, *Math. Sci.* **2018**, *12*, 205–210.
- [87] A. J. Bard, J. A. Crayston, G. P. Kittleson, T. V. Shea, M. S. Wrighton, *Anal. Chem.* **1986**, *58*, 2321–2331.
- [88] S. Ounnunkad, A. I. Minett, M. D. Imisides, N. W. Duffy, B. D. Fleming, C.-Y. Lee, A. M. Bond, G. G. Wallace, *J. Electroanal. Chem.* **2011**, *652*, 52–59.
- [89] K. J. Aoki, J. Chen, X. Zeng, Z. Wang, *RSC Adv.* **2017**, *7*, 22501–22509.
- [90] K. J. Aoki, J. Chen, P. Tang, *J. Phys. Chem. C* **2018**, *122*, 16727–16732.
- [91] K. J. Aoki, J. Chen, *Faraday Discuss.* **2018**, *210*, 219–234.

Accepted: March 3, 2020
Published online on March 24, 2020